SPE · AAPG · SEG
CCUS
Carbon Capture, Utilization, and Storage

CCUS: 4443516

Multiscale Analysis of Silica Nanoparticle Injection to Improve Long-Term CO_2 Injectivity

Doguhan Barlas Sevindik[1], Ryosuke Okuno[1], Hirotake Kitagawa[2], Md Fahim Shahriar[3], and Aaditya Khanal[4]
[1]The University of Texas at Austin, [2]Nissan Chemical Corporation, [3]The University of Texas at Tyler, [4]The University of Tulsa

Abstract

This study examines how altering wettability affects field-scale geologic CO_2 storage by injecting SiO_2 nanoparticles that modify the near-wellbore region to a strongly water-wet state. The objectives included experimentally measuring nanoparticle adsorption on quartz sands and changes in relative permeability during CO_2/water two-phase flow, as well as applying laboratory results to study CO_2 injectivity in field-scale simulations. Experiments used sandpacks made of Accusil quartz and compared untreated systems with nanoparticle-treated ones. Drainage and imbibition experiments yielded distinct relative permeabilities, confirming that nanoparticle adsorption altered wettability. The history-matched experimental results were then integrated into the Sleipner geological model using Corey's relative-permeability model. Simulation cases used varying injection amounts and concentrations to analyze the effects of nanoparticle injection on CO_2 injectivity. Applying the experimentally derived relative-permeability model to the site's original data showed that injecting 1.0 tonne of nanoparticles made the near-well region within 4.0 m of the injection well more water-wet, increasing CO_2 injectivity by 35%. Simulation results indicated that injectivity enhancements were primarily driven by wettability alteration, while the affected diameter played a secondary role.

Introduction

CCUS involves capturing CO_2 from various emission sources and storing it in deep geologic formations such as depleted hydrocarbon reservoirs, hydrothermal systems, deep coal seams, and saline aquifers (Bachu, 2015; Akin et al., 2025). These formations are estimated to provide a storage capacity of 8,000–55,000 $GtCO_2$, offering a substantial long-term mitigation pathway (Dooley, 2013; Bui et al., 2018). Among potential storage formations, saline aquifers are viewed as the most promising option because of their broad availability and storage capacity. Large-scale projects, including Sleipner, Snøhvit, Quest, and the Illinois

Basin Decatur Project, have stored millions of tonnes of CO_2, demonstrating the sustainability of CO_2 storage operations (Maldal and Tappel, 2004; Bachu and Gunter, 2004; Bourne et al., 2014; Finley, 2014).

Well injectivity in CO_2 storage is a vital parameter that controls injection timelines and operational costs. Injectivity depends primarily on petrophysical properties such as permeability and rock compressibility, as well as relative permeability and capillary pressure, both of which are directly controlled by the rock's wettability (Machado et al., 2023; Burton et al., 2008). There is no consensus regarding which wetting state favors CO_2 well injectivity. In strongly water-wet systems, well injectivity may be affected by salt precipitation and deposition caused by capillary-driven backflow near the well (André et al., 2014) and by fines migration and associated injectivity loss (Machado et al., 2023). The endpoint CO_2 relative permeability is particularly important; higher endpoints yield higher injectivity (Lee et al., 2009), which can be achieved in strongly water-wet systems. When salt precipitation is unlikely (NaCl solubility at 40 °C is approximately 36 g/100 mL), water-wet conditions tend to favor injectivity by increasing CO_2 mobility (Pinho and Macedo, 2004; Lee et al., 2009).

This study examined how wettability affects CO_2 well injectivity by injecting a SiO_2 nanoparticle solution as a wettability modifier. To the best of our knowledge, this is the first study to evaluate nanoparticle-induced changes in wettability to improve CO_2 injectivity. The study integrated sandpack experiments with field-scale simulations, tested multiple injection strategies, and extended earlier nanoparticle studies focused on CO_2 trapping to field-scale injectivity enhancements (Sevindik et al., 2025).

Experiments and Field-Scale Simulation Case Study

To assess the impact of SiO_2 nanoparticle injection, sandpack experiments (2.58 cm in diameter, 31.00 cm in length) were conducted without (Exp. #1) and with nanoparticle injection (Exp. #2) at a 0.50 wt.% concentration. The experiments were conducted under atmospheric conditions, so analog fluids were used, namely Soltrol 220 (density 787.0 kg/m^3, viscosity 4.43 mPa-s) and a glycerol/brine mixture (density 1117.0 kg/m^3, viscosity 4.35 mPa-s), to represent the CO_2–brine binary system under subsurface conditions (Sevindik et al., 2025). For each experiment, the corresponding relative-permeability curves were obtained through numerical history matching. To evaluate wettability, the modified Lak index (I_{ML}) was used, which increases with increasing water-wetness (Mirzaei-Paiaman et al., 2022). Key properties of the sandpack flooding experiments are given in Table 1.

Table 1. Summary of experimental cases and the sandpack properties. φ stands for porosity, S_{sr} stands for residual Soltrol 220 saturation, S_{irw} stands for irreducible water saturation, k_{rs} stands for Soltrol 220 relative permeability, and k_{rw} stands for water relative permeability.

Exp. #	U.S Sieve Fraction	Nanoparticle Treatment	φ	S_{sr}	S_{irw}	k_{rs} @ S_{irw}	k_{rw} @ S_{sr}	I_{ML}
1	20-30	-	0.42	0.226	0.348	0.572	0.560	-0.13
2		Done	0.40	0.223	0.262	0.886	0.430	+0.45

Furthermore, the field-scale simulations used the Sleipner CO_2 injection site's model, adopted from the Sleipner 2019 Benchmark Model (2020), covering an area of 3.2 × 5.9 km^2. The simulation domain was discretized into 64 × 118 × 74 grid blocks, with 25-fold grid refinement near the horizontal injector (86.2° inclination angle), resulting in a total of 624,774 grid blocks. The CMG GEM (GEM User Manual, 2024) was used to solve the conservation equations. The relative permeability of the brine-CO_2 system for the Utsira Formation (the target injection zone in the Sleipner project) was taken from Akervoll et al. (2009). The model was simulated for 10 years of CO_2 injection at an injection rate of one million tonnes per year.

To translate the wettability alteration observed in sandpack flooding experiments to the field scale, firstly, Corey's relative-permeability scaling was applied to estimate the altered relative-permeability curves for the Utsira Formation. Secondly, to account for varying nanoparticle concentrations and adsorption levels across the reservoir, an interpolation function was implemented to model intermediate wettability states as described in CMG STARS (STARS User Manual, 2024). The end-point relative permeability values for the CO_2-rich phase (k_{rg} @ S_{irw}) across different injection cases are given in Table 1.

The nanoparticle injection cases were grouped into three sets (Table 1). Cases 1–3 evaluated the effect of injection mass at a fixed concentration in the injection water (0.50 wt.%) using the experimental adsorption value of 17.44 mg-NP/100.0 g-rock. Note that 1.0 tonne (Case 1) was the minimum mass identified to alter wettability. Cases 4 and 5 used lower concentrations for the same injection mass as Case 2, assuming a linear relationship between injection concentration and nanoparticle adsorption (Hu et al., 2016). Moreover, those lower-concentration cases could introduce uncertainty about how adsorption translates into wettability alteration. Hence, additional cases for those injection concentrations were investigated (Cases 4-LW, 4-MW, 5-LW, and 5-MW) to account for the nonlinear relationship between adsorption amount and wettability alteration, which biased wettability toward being either more or less water-wet ("MW" or "LW" for Cases 4 and 5).

Table 1. Simulated cases to analyze the effect of nanoparticle injection amount, injection concentration, and nonlinear wettability alteration. For nonlinear wettability-alteration cases, LW and MW stand for the less and more water-wet conditions, respectively. Key results are presented as adsorption amounts, the Lak indexes, well injectivity (I), and the impacted diameter in the near-wellbore region.

Case #	Cumulative Injection tonnes	Concentration wt.%	Adsorption (mg-NP/100.0 g-rock)	k_{rg} @ S_{irw}	Lak Index	Average *I* m^3/d/kPa	Impacted Diameter m
Base	0.0	0.00	0.00	0.302	0.06	12.34	0.0
1	1.0	0.50	17.44	0.714	0.70	16.63	4.0
2	2.5	0.50	17.44	0.714	0.70	17.51	8.0
3	10.0	0.50	17.44	0.714	0.70	18.48	18.0
4	2.5	0.05	1.79	0.344	0.17	13.76	30.0
5	2.5	0.10	12.21	0.590	0.58	17.21	12.0
4-LW	2.5	0.05	1.79	0.303	0.07	12.64	30.0
4-MW	2.5	0.05	1.79	0.535	0.51	16.52	30.0
5-LW	2.5	0.10	12.21	0.401	0.30	14.51	12.0
5-MW	2.5	0.10	12.21	0.679	0.66	18.03	12.0

Results and Discussion

The results for the base case and Cases 1-3 are presented in Figure 1a, as the pressure propagation away from the wellbore from the middle completion interval of the horizontal injector along the y-direction. Dashed lines mark the nanoparticle-affected regions, within which the pressure gradient was approximately 1.75 kPa/m. This extended to diameters of 4.0, 8.0, and 18.0 meters across the cases. Beyond the affected zone, the pressure gradient increased by approximately 26% to 2.20 kPa/m. In combination with the reduced pressure gradient and the extent of the wettability-alteration zone, these effects directly influenced the pressure propagation and the well bottom-hole pressures (P_{bhp}) as shown in Figure 1b.

Figure 1b shows the simulated P_{bhp} histories. Cases 1–3 had similar P_{bhp} values because wettability alteration occurred in each case within the near-wellbore region (about 4.0, 8.0, and 18.0 meters), which was sufficient to lower the pressure buildup. This pattern was driven by a rapid reduction in water saturation in the near-wellbore: as CO_2 was injected, water saturation quickly dropped to irreducible levels, after which the endpoint CO_2 relative permeability controlled the P_{bhp} response (Table 1). Differences among cases arose from the extent of nanoparticle spread, where well injectivity was enhanced relative to the base case.

Figure 2 presents simulation results for cases that vary in injection concentration and in the degree of nonlinearity between adsorption and wettability alteration. The error bars span from the LW cases at the bottom of the bars to the MW cases at the top. The data suggest that a 0.05 wt.% injection concentration produced minimal enhancement in injectivity unless the wettability shift favored a more water-wet condition than observed in the experiments. Even then, the increase in well injectivity did not exceed the improvement seen with 0.50 wt.%. Conversely, a 0.10 wt.% injection concentration significantly improved well injectivity, matching the 0.50 wt.% enhancement level. Additionally, if wettability shifted toward a less water-wet state, a 17.6% increase in injectivity would still be observed.

The mechanism that enhanced injectivity was the combined effect of near-wellbore nanoparticle adsorption and the extent of the wettability-alteration zone. Both parameters promoted injectivity; however, higher

injection concentrations increased adsorption, which limited nanoparticle spreading and reduced the extent of the stimulated zone. A 0.10 wt.% injection concentration balanced these two factors, yielding an adsorption of 12.21 mg-NP/100.0 g-rock and an affected diameter of 12.0 m around the well. Lower injection concentrations, such as 0.05 wt.%, were unlikely to be effective unless the wettability alteration associated with nanoparticle adsorption was heavily biased toward a strongly water-wet state.

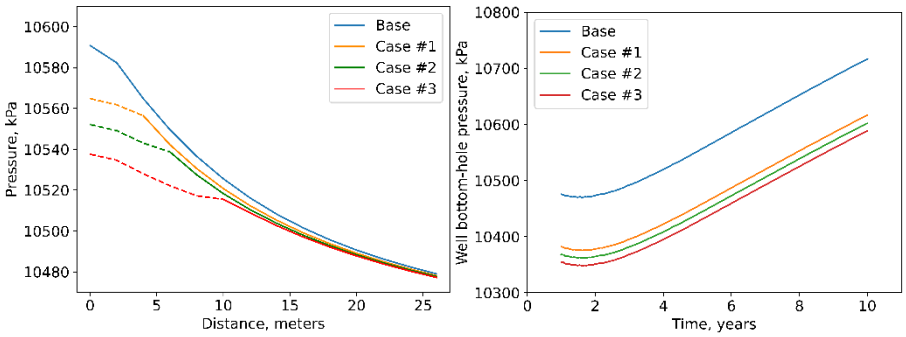

Figure 1. Results of the nanoparticle injection cases varying on injection mass (Cases 1-3, Table 1); (a) Pressure profiles away from the wellbore (the well at 0 m), constructed from the x-y cross-section at completion depth for the simulated cases after 10 years of CO_2 injection. Dashed lines represent the wettability-alteration zone; (b) P_{bhp} for the simulated cases for the CO_2 injection period.

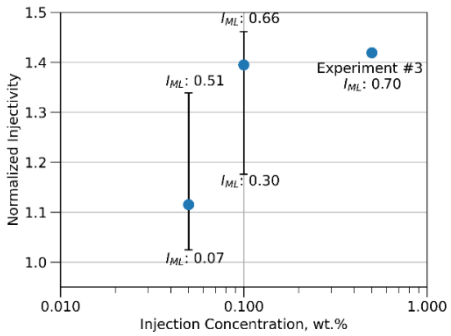

Figure 2. Results of the impact of injection concentration on well injectivity. The y-axis represents the normalized injectivity relative to the base case, and the x-axis represents the injection concentration in wt.% on a log scale. I_{ML} stands for modified Lak index.

In Figure 3, a range of formation water wetness, measured by the I_{ML}, is shown for rock samples (red dots) from major sandstone saline aquifers that have stored CO_2 (Shi et al., 2013; Bauer et al., 2019; Bachu et al., 2013; Reynolds and Krevor, 2015). The original state of the Utsira formation, the experimental data, and field-scale simulations at different concentrations are shown by yellow dots. This figure shows that injectivity increased with higher water-wetness (Table 1, Figures 1-2). It is beneficial to assess the wetting state of aquifers beforehand. This helps determine whether a wettability modifier could be used to improve well injectivity, while accounting for uncertainties specific to the target formation.

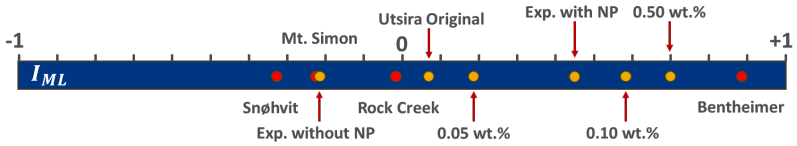

Figure 3. Calculated I_{ML} for sandstone saline aquifers (red dots) and the experiments/simulations involving different concentrations (yellow dots).

Conclusions

This study investigated the potential of SiO_2 nanoparticles as a wettability modifier to improve CO_2 injectivity by combining sandpack flooding experiments with field-scale numerical simulations. Results showed that injecting at least 1.0 tonne of nanoparticles increased CO_2 injectivity by more than 35% and that injecting larger amounts expanded the wettability-alteration zone around the wellbore, producing smaller pressure gradients farther into the formation. While nanoparticle concentration strongly controlled injectivity enhancement, dilute injections spread more widely with relatively minor wettability alteration. The degree of water wetness was the primary driver of injectivity improvement, whereas the impacted diameter played a secondary role.

Acknowledgements

This research was conducted as part of the Energi Simulation Industrial Affiliate Program on Sustainable Energy Expansion at The University of Texas at Austin (UT Austin). The authors thank Nissan Chemical Corporation for providing nanoparticle samples. AK and MFS acknowledge the U.S. Department of Energy, Office of Science, Basic Energy Sciences Geoscience program under Award Number DE-SC0025695. Any opinions, findings, and conclusions or recommendations expressed in this material are those of the author(s) and do not necessarily reflect the views of the funding agency. Ryosuke Okuno holds the H. B. (Burt) Harkins, Jr. Professorship in Petroleum Engineering at UT Austin.

References

Akervoll, I., E. Lindeberg, and A. Lackner, 2009, Feasibility of Reproduction of Stored CO_2 from the Utsira Formation at the Sleipner Gas Field: Energy Procedia, v. 1, no. 1, p. 2557–2564, doi:10.1016/j.egypro.2009.02.020.

Akın, T., S. Erol, A. B. Tokel, D. B. Sevindik, and S. Akın, 2025, Monitoring CO_2 Injection in the Kızıldere Geothermal Field: International Journal of Greenhouse Gas Control, v. 146, p. 104413, doi:10.1016/j.ijggc.2025.104413.

André, L., Y. Peysson, and M. Azaroual, 2014, Well injectivity during CO_2 storage operations in deep saline aquifers – Part 2: Numerical simulations of drying, salt deposit mechanisms and role of capillary forces: International Journal of Greenhouse Gas Control, v. 22, p. 301–312, doi:10.1016/j.ijggc.2013.10.030.

Bachu, S., 2013, Drainage and Imbibition CO_2/Brine Relative Permeability Curves at in Situ Conditions for Sandstone Formations in Western Canada: Energy Procedia, v. 37, p. 4428–4436, doi:10.1016/j.egypro.2013.07.001.

Bachu, S., 2015, Review of CO_2 storage efficiency in deep saline aquifers: International Journal of Greenhouse Gas Control, v. 40, p. 188–202, doi:10.1016/j.ijggc.2015.01.007.

Bachu, S., and W. D. Gunter, 2004, Acid-gas injection in the Alberta Basin, Canada: A CO_2 storage experience: Geological Society, London, Special Publications, v. 233, no. 1, p. 225–234, doi:10.1144/gsl.sp.2004.233.01.15.

Bauer, R. A., R. Will, S. E. Greenberg, and S. G. Whittaker, 2019, Illinois Basin–Decatur project: Geophysics and Geosequestration, p. 339–370, doi:10.1017/9781316480724.020.

Bourne, S., S. Crouch, and M. Smith, 2014, A risk-based framework for measurement, monitoring and verification of the Quest CCS Project, Alberta, Canada: International Journal of Greenhouse Gas Control, v. 26, p. 109–126, doi:10.1016/j.ijggc.2014.04.026.

Bui, M. et al., 2018, Carbon capture and storage (CCS): The way forward: Energy & Environmental Science, v. 11, no. 5, p. 1062–1176, doi:10.1039/c7ee02342a.

Burton, M., N. Kumar, and S. L. Bryant, 2008, Time-dependent Injectivity During CO_2 Storage in Aquifers: SPE Symposium on Improved Oil Recovery, doi:10.2118/113937-ms.

Computer Modeling Group (CMG). 2024. GEM User Manual. Computer Modeling Group (CMG).

Computer Modeling Group (CMG). 2024. STARS User Manual. Computer Modeling Group (CMG).

Dooley, J. J., 2013, Estimating the Supply and Demand for Deep Geologic CO_2 Storage Capacity over the Course of the 21^{s}t Century: A Meta-analysis of the Literature: Energy Procedia, v. 37, p. 5141–5150, doi:10.1016/j.egypro.2013.06.429.

Finley, R. J., 2014, An overview of the Illinois Basin – Decatur Project: Greenhouse Gases: Science and Technology, v. 4, no. 5, p. 571–579, doi:10.1002/ghg.1433.

Hu, Z., S. M. Azmi, G. Raza, P. W. Glover, and D. Wen, 2016, Nanoparticle-Assisted Water-Flooding in Berea Sandstones: Energy & Fuels, v. 30, no. 4, p. 2791–2804, doi:10.1021/acs.energyfuels.6b00051.

Lee, Y. S., K. H. Kim, T. H. Lee, W. M. Sung, Y. C. Park, and J. H. Lee, 2009, Analysis of CO_2 Endpoint Relative Permeability and Injectivity by Change in Pressure, Temperature, and Phase in Saline Aquifer: Energy Sources, Part A: Recovery, Utilization, and Environmental Effects, v. 32, no. 1, p. 83–99, doi:10.1080/15567030903077337.

Machado, M. V., M. Delshad, and K. Sepehrnoori, 2023, Injectivity assessment for CCS Field-scale projects with considerations of salt deposition, mineral dissolution, fines migration, hydrate formation, and non-Darcy Flow: Fuel, v. 353, p. 129148, doi:10.1016/j.fuel.2023.129148.

Maldal, T., and I. M. Tappel, 2004, CO_2 underground storage for Snøhvit gas field development: Energy, v. 29, no. 9–10, p. 1403–1411, doi:10.1016/j.energy.2004.03.074.

Mirzaei-Paiaman, A., M. Faramarzi-Palangar, S. Djezzar, and S. Kord, 2022, A new approach to measure wettability by relative permeability measurements: Journal of Petroleum Science and Engineering, v. 208, p. 109191, doi:10.1016/j.petrol.2021.109191.

Pinho, S. P., and E. A. Macedo, 2004, Solubility of NaCl, NaBr, and KCl in Water, Methanol, Ethanol, and Their Mixed Solvents: Journal of Chemical & Engineering Data, v. 50, no. 1, p. 29–32, doi:10.1021/je049922y.

Reynolds, C. A., and S. Krevor, 2015, Characterizing flow behavior for gas injection: Relative permeability of CO_2-brine and N_2-water in heterogeneous rocks: Water Resources Research, v. 51, no. 12, p. 9464–9489, doi:10.1002/2015wr018046.

Sevindik, D. B., H. Ni, R. Okuno, and H. Kitagawa, 2025, Impact of Wettability on CO_2 Plume Migration and Trapping: Sand-Tank Experimentation and Modeling: SPE Annual Technical Conference and Exhibition, doi:10.2118/228184-ms.

Shi, J.-Q., C. Imrie, C. Sinayuc, S. Durucan, A. Korre, and O. Eiken, 2013, Snøhvit CO_2 Storage Project: Assessment of CO_2 Injection Performance Through History Matching of the Injection Well Pressure Pver a 32-months Period: Energy Procedia, v. 37, p. 3267–3274, doi:10.1016/j.egypro.2013.06.214.

Sleipner 2019 Benchmark Model, 2020, doi.org:10.11582/2020.00004.